A theoretical model of the pressure field arising from asymmetric intraglottal flows applied to a two-mass model of the vocal folds

Byron D. Erath[a)]
Department of Mechanical and Aerospace Engineering, The George Washington University, Washington, DC 20052

Sean D. Peterson
Department of Mechanical and Mechatronics Engineering, University of Waterloo, Waterloo, ON N2L 3G1, Canada

Matías Zañartu[b)]
School of Electrical and Computer Engineering, Purdue University, West Lafayette, Indiana 47907

George R. Wodicka[c)]
Weldon School of Biomedical Engineering, Purdue University, West Lafayette, Indiana 47907

Michael W. Plesniak
Department of Mechanical and Aerospace Engineering, The George Washington University, Washington, DC 20052

(Received 2 April 2010; revised 25 February 2011; accepted 12 April 2011)

A theoretical flow solution is presented for predicting the pressure distribution along the vocal fold walls arising from asymmetric flow that forms during the closing phases of speech. The resultant wall jet was analyzed using boundary layer methods in a non-inertial reference frame attached to the moving wall. A solution for the near-wall velocity profiles on the flow wall was developed based on a Falkner-Skan similarity solution and it was demonstrated that the pressure distribution along the flow wall is imposed by the velocity in the inviscid core of the wall jet. The method was validated with experimental velocity data from 7.5 times life-size vocal fold models, acquired for varying flow rates and glottal divergence angles. The solution for the asymmetric pressures was incorporated into a widely used two-mass model of vocal fold oscillation with a coupled acoustical model of sound propagation. Asymmetric pressure loading was found to facilitate glottal closure, which yielded only slightly higher values of maximum flow declination rate and radiated sound, and a small decrease in the slope of the spectral tilt. While the impact on symmetrically tensioned vocal folds was small, results indicate the effect becomes more significant for asymmetrically tensioned vocal folds. © *2011 Acoustical Society of America*. [DOI: 10.1121/1.3586785]

PACS number(s): 43.70.Aj, 43.70.Bk, 43.70.Jt [CHS] Pages: 389–403

I. INTRODUCTION

Voiced speech involves complex fluid-structure interactions that occur within the larynx. In preparation for speech, the vocal folds are adducted and pressure increases within the lungs until it becomes great enough to overcome the elastic closing force of the vocal folds. As air is forced through the glottis (the opening between the vocal folds) the resulting aerodynamic pressures coupled with the material properties of the vocal fold tissue initiate self-sustained oscillations of the vocal folds.[1]

The basic mechanics of vocal fold motion during speech are well understood,[2] with each repeating phonatory cycle creating a temporally-varying glottal geometry, shown schematically in Fig. 1. Initially, the vocal folds are in contact, as shown in Fig. 1, tile 1. As the vocal folds are pushed apart by the subglottal pressure, the glottis forms a convergent channel with the phase of the inferior portion of the medial vocal fold wall leading the superior portion (tile 2). As the cycle progresses, the vocal folds reach maximal opening, forming a uniform channel within the glottis (tile 3). While closing, the glottis forms a divergent passage, again due to the phase lag between the inferior and superior surfaces (tile 4), before returning to its initial position (tile 1).

The importance of the pressure-flow relationship within the glottis has long been realized, as evidenced by early experimental investigations.[3] Consequently, considerable effort has been placed on first identifying intraglottal flow behavior and then ascertaining its influence on the energy exchange process. Good progress was made in developing pressure-flow relationships for speech in early steady flow investigations through static vocal fold models.[4–6] However, these investigators did not visualize the flow and therefore did not detect the flow structures. It was not until the work of Teager,[7] Teager and Teager,[8,9] and Kaiser[10] that flow

[a)]Author to whom correspondence should be addressed. Electronic mail: erath@gwu.edu
[b)]Present address: Department of Electronic Engineering, Universidad Técnica Federico Santa María, Av. España 1680, Valparaíso, Chile.
[c)]Also at: School of Electrical and Computer Engineering, Purdue University, West Lafayette, IN 47907.

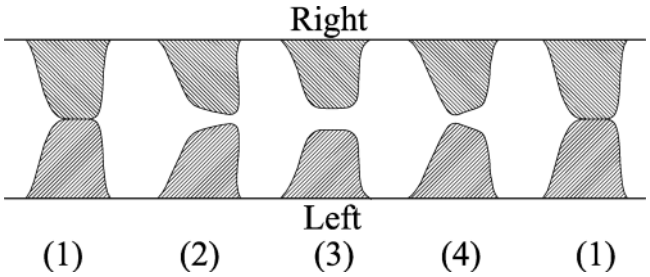

FIG. 1. Schematic of the glottal geometry showing the left and right vocal folds throughout one phonatory cycle. (1) Closed, (2) Convergent passage, (3) Uniform passage, (4) Divergent passage, (1) Closed.

asymmetries in speech were first proposed. Subsequent investigations explored impulsively started flow through three times life-sized vocal fold models.[11–14] The formation of asymmetric flow (the Coanda effect)[15] in the glottis was conceded, but it was postulated that scaling the time in order to account for the larger model size would preclude the development of asymmetric flows *in vivo*.

Contrary to the proposed hypothesis that viscous phenomena require a large time scale to develop, spatial reconstruction of the supraglottal flow field in excised canine larynges using hotwire anemometry suggested an asymmetry, or skewing, of the glottal flow.[16–18] These findings were consistent with the formation of the Coanda effect. In more recent investigations, fully-pulsatile flow through 7.5 times life-sized vocal fold models was investigated.[19,20] Phase-averaged Particle Image Velocimetry (PIV) was used to measure highly-resolved spatial velocity fields at discrete instances throughout the phonatory cycle. Asymmetric flow configurations were consistently present during the divergent portions of the cycle due to the formation of the Coanda effect. It was shown that the formation of the Coanda effect was dependent upon the acceleration of the flow, and furthermore, had sufficient time to develop during phonation.[19–21] Similar flow asymmetries have been observed in both static,[22–24] and increasingly complex vocal models, including flow through dynamically-driven models,[25–30] self-oscillating models,[31–33] and excised canine larynges.[34] In addition to visualizing flow asymmetries, steady flow investigations through static vocal fold models quantitatively identified large cross-channel pressure asymmetries between the vocal fold walls caused by the asymmetric attachment of the glottal jet to one vocal fold wall.[22–24] While these investigations have provided a more accurate description of the intraglottal flow field, a quantitative description of the impact of flow asymmetries on dynamic vocal fold biomechanics and the radiated sound field has yet to be determined.

An attractive alternative to experimental flow investigations is lumped-mass models, which were developed as an effective tool for investigating fluid-structure and flow-sound interactions during speech. The appeal of lumped-mass models is their ability to efficiently and economically model the energy exchange process within the larynx. Initially proposed as a single spring-mass-damper system,[35] and later expanded to two masses in order to capture phase differences between the inferior and superior portions of the vocal folds,[36] lumped-mass models are now ubiquitous in the speech literature for investigating both normal and pathological speech conditions.[37–42] However, in order to ensure their relevance, accurate models of both the flow and tissue properties are required.

Despite recent advances in laryngeal flow investigations, virtually all lumped-mass models of phonation continue to approximate the fluid mechanics using the Bernoulli equation,[43–46] a method that has remained relatively unchanged since it was first proposed as a glottal flow model over 50 years ago.[47] Describing the flow field with the Bernoulli equation assumes the fluid behaves throughout the phonatory cycle in a one-dimensional, steady, inviscid manner along an identifiable streamline, a gross simplification of actual reported behavior. Further confusing the matter, most lumped-mass models simply assume that the Bernoulli equation is applicable up to some predetermined location of flow separation, whereupon the flow symmetrically separates from both vocal fold walls. The separation point in the divergent glottis is typically defined at a location where the ratio of glottal area to minimal glottal area ($a_{\text{glottis}}/a_{\text{min}}$) is equal to a predetermined constant. Although it was initially proposed that the flow separates at an area ratio of 1.2, values of 1.0, and 1.1 have also been employed.[12,42,46,48–50] Aside from the disquieting aspect of prescribing a fixed flow separation location, this method fails to adequately describe the intraglottal flow asymmetries that arise during the closing phases of the phonatory cycle.[19,20,25–27,30,51] Were it appropriate to assume that the flow is symmetric, the issue remains that the divergent glottal area generates an adverse pressure gradient that results in significant boundary layer growth, thereby violating the assumption of inviscid flow that is requisite for using the Bernoulli equation. Consequently, the validity of lumped-mass model investigations are limited by their inability to economically implement an adequate flow solution that is capable of capturing the relevant flow physics. To overcome some of these issues, many models implement *ad hoc* assumptions that have no physical basis in an attempt to compensate for the shortcomings of the Bernoulli equation.[47]

Asymmetric flow effects have yet to be introduced in lumped-mass models due to the lack of a theoretical solution that bridges the gap between experimental observations and practical implementation. In this paper, a theoretical model is proposed for the asymmetric pressure distribution encountered by the vocal fold walls during the divergent portion of the phonatory cycle (see tile 4 of Fig. 1), during which the glottal jet is attached to one wall. Attachment of the glottal jet to one wall via a Coanda-type effect tends to occur when the total included angle of the vocal folds is less than -6 to $-8°$.[52,53] Throughout the manuscript the glottal angle is defined such that positive values correspond to convergent angles, and negative values correspond to divergent angles. The pressure along the flow wall, that is, the wall to which the glottal jet is attached, is estimated via a boundary layer analysis, while the pressure on the non-flow wall is assumed to be fully-separated, and thus equal to the pressure at the exit of the glottis (typically modeled as atmospheric pressure). The proposed Boundary Layer Estimation of Asymmetric Pressure (BLEAP) scheme is a closed-form solution,

allowing seamless integration into existing lumped-mass model formulations.

The paper is organized as follows. The theoretical aspects of the flow model are presented in Sec. II, including introduction to the free parameters to be assessed from experiments. The requisite experiments, estimation of the free parameters, and scheme implementation are discussed in Sec. III. The proposed method is applied to a standard two-mass model for self sustained vocal fold oscillations in Sec. IV and Sec. V is left for the conclusions.

II. THEORY

As previously discussed, the majority of glottal flow solvers employ the 1-D, invisicid, Bernoulli equation to describe the entire glottal flow field and thereby solve the pressures that drive vocal fold motion. During the converging phases of the phonatory cycle this model is expected to be accurate as the pressure gradient is favorable and the boundary layers on the vocal fold walls are thin. However, it is known that during the phases of the phonatory cycle in which the walls diverge, boundary layer growth is appreciable, flow separation can occur, symmetry can be broken, and the glottal jet can attach to one wall or the other, thereby violating the underlying assumptions of a Bernoulli flow solver. In this section an alternate model for the intraglottal pressure is proposed that is capable of describing the aforementioned intraglottal flow physics. The new theoretical model is based upon a similarity solution derived from a boundary layer analysis that assumes the glottal jet is attached to one wall and completely separated from the other. Similarity solutions are attractive because they reduce the number of independent variables, thereby reducing the governing equations from partial differential equations to tractable ordinary differential equations, while still maintaining the integrity of the governing equations that describe the flow behavior. In order to find a similarity solution, the mapping must not only reduce the governing equations to a set of ordinary differential equations, but also successfully transform the boundary conditions to finite-valued constraints.[54] The motivation for employing this approach is to determine a theoretical flow solution that predicts the pressure loadings on the vocal folds arising from asymmetric intraglottal flows. Unlike an empirical approach, this mathematical transformation ensures the solution is broadly applicable to speech.

A. Flow model description and governing equations

The medial surfaces of the vocal folds during the diverging portion of the phonatory cycle are modeled to first order as two translating and rotating semi-infinite flat plates. The flow is assumed to be attached to one wall and completely separated from the other, with separation from the non-flow wall occurring at the minimal glottal area. The fluid motion along the flow wall is modeled as a quasi-steady wall jet, which can in turn be modeled using boundary layer methods.[55] The pressure distribution along the non-flow wall is assumed to be atmospheric. Pressure recovery has been observed along the non-flow wall in experimental static, steady flow investigations,[22–24] but the amount of recovery is very small in comparison to the pressure recovery that occurs along the flow wall, and thus is neglected. Furthermore, invoking the assumption of constant pressure downstream of the point of separation allows direct comparison with existing multi-mass model investigations that employ this same simplification. The pressure along the flow wall arising from the asymmetric jet attachment is unknown and will be determined in the following analysis. All future references to the wall (or plate) will be assumed to be the flow wall, unless specifically stated otherwise. It is noted that the pressure need not be constant in a given cross section of the passage since the velocity is not everywhere perpendicular to the cross-section plane.

An inertial coordinate system XYZ is defined to be fixed relative to the larynx, where X corresponds to the streamwise, or superior, direction, Y is in the medial/lateral direction and is oriented from the left to right vocal fold (see Fig. 1), and Z completes the standard right-handed coordinate system and points in the anterior direction (see Fig. 2). The unit vectors pointing in the X, Y, and Z-directions are $\hat{I}$, $\hat{J}$, and $\hat{K}$, respectively. The vocal fold wall is modeled as a flat plate with the leading edge corresponding to the fixed X position of the minimum glottal area, which is set as 0. A body-fixed coordinate system that moves with the vocal fold wall is denoted xyz, where x is along the length of the plate in the streamwise direction, y is the wall-normal direction, and z has the same orientation as Z. The body-fixed coordinate system has unit vectors $\hat{i}$, $\hat{j}$, and $\hat{k}$ in the x, y, and z directions, respectively. The position of the leading edge of the plate with respect to the fixed coordinate system is given by $\vec{R}(t) = |\vec{R}(t)|\hat{J}$, where $|\vec{R}(t)|$ is the magnitude of the displacement, which is confined to the Y direction. Thus, the leading edge of the plate has a varying Y position, but X is fixed at 0. Note that when pointing to the left wall $\vec{R}(t)$ is pointing in the $-\hat{J}$ direction. The plate rotates about the z axis with angular velocity $\vec{\Omega}(t) = \Omega_z(t)\hat{k}$, where the magnitude $\Omega_z(t)$ can be either positive or negative, depending on the phonation phase. The translation and rotation of the plate are shown schematically in Fig. 2.

The air flowing over the vocal fold wall is modeled as an incompressible, Newtonian fluid. Therefore, the fluid motion is governed by the Navier-Stokes equations, which represent conservation of mass and momentum. In an inertial reference frame, these equations are

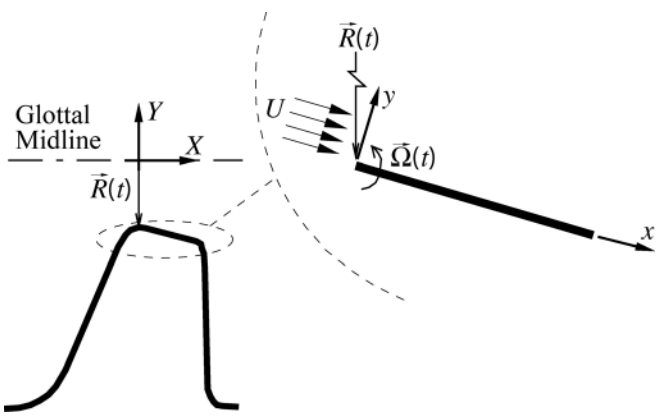

FIG. 2. Schematic of a simplified model of a vocal fold represented by a translating and rotating flat plate.

$$\nabla \cdot \vec{V}_{XYZ} = 0, \tag{1a}$$

$$\rho\left[\frac{\partial \vec{V}_{xyz}}{\partial t} + \left(\vec{V}_{xyz} \cdot \nabla \vec{V}_{xyz}\right)\right] = \rho\vec{g} - \nabla p + \mu\nabla^2\vec{V}_{xyz}, \tag{1b}$$

where $\vec{V}$ is the velocity field, ρ is the fluid density, μ is the dynamic fluid viscosity, $\vec{g}$ is gravity, p is the pressure, ∇ is the gradient operator, t is time, and the subscript XYZ indicates that the variable is with respect to the inertial XYZ frame.

In the inertial frame, the boundary conditions are nonhomogenous and time-dependent. This complexity is eliminated by writing Eqs. (1a) and (1b) in the non-inertial body-fixed frame, which satisfies the requirement of the similarity solution that the boundary conditions be finite valued. In the body-fixed frame, the boundary conditions are $u(x,y=0)=v(x,y=0)=0$, where u and v are the x and y velocity components, respectively, and the z component of velocity is zero by definition. These boundary conditions correspond to the standard no-slip and no-penetration boundary conditions for solid surfaces.

Converting from the inertial to non-inertial reference frame introduces fictitious forces due to the relative motion of the body-fixed reference frame xyz with respect to the fixed frame XYZ.[56] Assuming constant linear and angular plate velocity magnitudes as a first order approximation of the vocal fold wall dynamics, neglecting gravity, and assuming a steady glottal jet, Eq. (1b) in the non-inertial frame becomes

$$\rho\left[\left(\vec{V}_{xyz} \cdot \nabla\right)\vec{V}_{xyz} + \vec{\Omega} \times \vec{\Omega} \times \vec{r}_{xyz} + 2\vec{\Omega} \times \vec{V}_{xyz}\right] = -\nabla p + \mu\nabla^2\vec{V}_{xyz}, \tag{2}$$

where the second and third terms in the brackets are the centripetal and Coriolis forces, respectively. Note that conservation of mass is independent of the coordinate system and thus remains unchanged.

From this point further, all references to velocity will refer to the non-inertial frame unless otherwise specified. In accordance, the subscript xyz is excluded in the remainder of the manuscript.

B. Scaling arguments and flow model development

1. Streamwise momentum

To elucidate the flow physics and to simplify the governing flow equations, classical scaling arguments are implemented, using the plate length L as the characteristic length, the velocity in the inviscid jet core U as the velocity scale (analogous in boundary layer theory to the free stream velocity), and δ as the distance from the wall to the location where the wall jet achieves $0.99U$ (analogous to a boundary layer thickness). Substituting these scaling factors into Eq. (1b) and considering only the x direction yields

$$u^*\frac{\partial u^*}{\partial x^*} + v^*\frac{\partial u^*}{\partial y^*} - \Lambda^2 x^* - 2\Lambda\delta^* = -\frac{\partial p^*}{\partial x^*} + \frac{1}{\mathrm{Re}}\left(\frac{\partial^2 u^*}{\partial x^{*2}} + \frac{1}{\delta^{*2}}\frac{\partial^2 u^*}{\partial y^{*2}}\right), \tag{3}$$

where the superscript * denotes a dimensionless variable, e.g., $\delta^* = \delta/L$, $\mathrm{Re} = \rho UL/\mu$ is the Reynolds number and $\Lambda = \Omega_z L/U$ is a dimensionless plate tip speed. Assuming the boundary layer thickness is significantly smaller than the plate length, that is, $\delta^* \ll 1$, then $(\partial^2 u^*/\partial y^{*2}) \gg (\partial^2 u^*/\partial x^{*2})$ and the latter viscous term can be neglected. Invoking standard boundary layer arguments by positing that the viscous terms should be of the same order as the inertial and pressure terms suggests that $\mathrm{Re} \sim O(1/\delta^{*2})$.[56] The final form of the momentum equation in the x direction depends on the scale of Λ, the three cases of which can be summarized as

$$\Lambda \sim O(\delta^*);\ \Lambda \sim O(1/\delta^*);\ \Lambda \sim O(1), \tag{4}$$

which correspond to $\Lambda \ll 1$, $\Lambda \gg 1$, and $\Lambda \sim O(1)$, respectively. Using a frequency range for speech of 120–275 Hz, an open quotient range of 0.4–1.0, a speed quotient range of 0.7–1.5, a transglottal pressure drop range of 3–15 cm H_2O,[57] a glottal length of 0.3 cm, and a divergent half angle during glottal closure of -10 to $-20°$,[22] Λ is computed to range from 0.004–0.163. Note that throughout the manuscript "glottal length" refers to the length of the medial vocal fold surface in the inferior-superior flow direction (x direction in Fig. 2) rather than the anterior-posterior direction. An estimate of the boundary layer thickness is $\delta^* \sim 0.01$,[25] which places Λ between $O(\delta^*)$ and $O(1)$. When $\Lambda \sim O(\delta^*)$ the governing equations reduce to the traditional steady, laminar boundary layer equations. As the magnitude of Λ increases toward unity, the centripetal term becomes relevant while the Coriolis term remains negligibly small. Given the range of potential values of Λ in speech, the centripetal terms are retained herein, while the Coriolis terms are neglected.

Neglecting the Coriolis term, the dimensional x momentum equation reduces to

$$u\frac{\partial u}{\partial x} + v\frac{\partial u}{\partial y} - x\Omega_z^2 = -\frac{1}{\rho}\frac{\partial p}{\partial x} + \nu\frac{\partial^2 u}{\partial y^2}, \tag{5}$$

where $\nu = \rho/\mu$. This equation is identical to the traditional boundary layer equation with the exception of the additional centripetal force term, which can be absorbed into the pressure term by defining a modified pressure $\tilde{p}$ as

$$\tilde{p} = p - \frac{1}{2}\rho x^2\Omega_z^2. \tag{6}$$

Differentiating Eq. (6) and incorporating it into Eq. (5) results in a modified version of the standard boundary layer formulation where the pressure gradient is influenced by the wall rotation as

$$u\frac{\partial u}{\partial x} + v\frac{\partial u}{\partial y} = -\frac{1}{\rho}\frac{\partial \tilde{p}}{\partial x} + \nu\frac{\partial^2 u}{\partial y^2}. \tag{7}$$

This is the final form of the governing equation for momentum in the x direction. Note that no simplifying assumptions regarding the viscous nature of the flow have been made. It can be shown that if the plate rotates about some point x_0 as opposed to the leading edge, the governing equation is

unchanged with the exception that the centripetal term in the modified pressure gradient is $\rho\,(x - x_0)\,\Omega_z^2$.

Qualitatively, expressing the centripetal acceleration in terms of the modified pressure has interesting implications on the flow separation characteristics of attached glottal jets. For instance, when no external pressure gradient is applied, that is, $\partial p/\partial x = 0$, the modified pressure gradient $\partial \tilde{p}/\partial x$ is positive for $x < x_0$, and negative for $x > x_0$. This signifies that downstream of the point of rotation, the surface rotation will act as a favorable pressure gradient and postpone separation. The favorable pressure gradient occurs regardless of the direction of rotation. This suggests that once the glottal jet attaches to the rotating wall, the wall rotation provides a stabilizing effect on the wall jet, thus delaying flow separation. This helps to explain why experimental studies show flow attachment at divergence angles that exceed the post-critical "diffuser" stall angle when the wall is rotating.[25,27]

2. Wall-normal momentum

In order to solve for the pressure along the flow wall in the non-inertial reference frame, the wall-normal pressure gradient within the boundary layer must be zero (to at least second order), allowing the free stream pressure gradient to be imposed upon the wall. Using the same scaling arguments of Sec. II.B.1 it can be shown that the y component of Eq. (2) reduces to $\partial p/\partial y = 0$ for $\Lambda \sim O\,(\delta^*)$ and $\Lambda \sim O\,(1)$. Thus, the pressure on the wall is equal to the pressure at the edge of the boundary layer, that is, in the free stream.

The relationship between the core velocity of the wall jet and the streamwise pressure gradient is estimated by assuming the jet core to be inviscid. Thus, the free steam flow is governed by Euler's equation in Cartesian coordinates with the inclusion of the corrective centripetal and Coriolis terms for the rotating reference frame. Assuming the free stream flow direction is parallel to the plate, that is, $\vec{V} = U\hat{\imath}$, where U is the free stream velocity magnitude, Euler's equation can be simplified to show

$$U\frac{dU}{dx} = -\frac{1}{\rho}\frac{\partial p}{\partial x} + x\Omega_z^2. \tag{8}$$

Note that when the streamlines are parallel to the moving plate, there is no contribution from the Coriolis force in the velocity-pressure relationship. Further note that the right hand side of Eq. (8) can be written using the derivative form of the modified pressure gradient of Eq. (6). The y pressure gradient is unimportant as only the pressure gradient in the x direction, and not the actual pressure magnitudes in the boundary layer, is of interest. Although the assumption that streamlines are parallel to the plate is not rigorously validated, it is expected that small deviations from this behavior will have a negligible influence on the streamwise pressure gradient.

C. Similarity solution

Expressing Eq. (8) in terms of a modified pressure and substituting it into Eq. (7) yields the governing equation and boundary conditions for the flow in the boundary layer. The resulting formulation is of the same form as the traditional boundary layer equation, and can therefore be solved using the approach of a Falkner-Skan similarity solution,[56,58] which requires that the free stream velocity develops as

$$U(x) = (c_1 x + c_2)^n, \tag{9}$$

where c_1, c_2, and n are constants.[54] The similarity variable is expressed as

$$\eta = y\sqrt{\frac{U'}{\beta\nu}} \tag{10}$$

with the prime indicating differentiation with respect to x, and

$$\beta = \frac{2n}{(n+1)}. \tag{11}$$

The constant β is related to the pressure gradient, with positive values of β indicating a negative, or favorable, pressure gradient. Negative values of β denote an adverse pressure gradient. Thorough discussions of the Falkner-Skan solutions and associated applications can be found in graduate fluid mechanics texts.[56,59]

III. FREE PARAMETER ESTIMATION AND FLOW MODEL IMPLEMENTATION

In order to ascertain the validity of the similarity solution for speech, the decay of the maximum glottal jet velocity can be evaluated to ensure that it meets the criterion of Eq. (9). In particular, in order to meet the requirements, the constants c_1 and c_2 must be positive, and $n > -0.0904$. The applicability of the theoretical solution to speech can be determined by extracting the free stream velocity from experimental data and determining whether a sufficient fit of the free parameters c_1, c_2, and n can be found that satisfies Eq. (9). If the fit is good, then the validity of the similarity solution is confirmed for the defined vocal fold motion.

A. Experimentally-measured velocity fields

The spatial variation in the maximum glottal jet velocity is extracted within the glottis from phase-averaged PIV data presented in Erath and Plesniak.[26] Data were acquired in 7.5 times life-sized, dynamically driven vocal fold models. Vocal fold motion was generated by simultaneously prescribing a linear and rotational component of motion for each vocal fold wall, which were driven by independent stepper motors/drivers. The motion approximated the mucosal wave to the first order, capturing the temporally varying geometry of normal vocal fold motion. Data were acquired at four discrete instances in the divergent portion of the phonatory cycle for three life-sized volumetric flow rates of $Q_{\text{mean}} = 0.089$, 0.159, and 0.253 L/s. 525 PIV image pairs were obtained at $t/T_{\text{open}} = 0.60$, 0.70, 0.80, and 0.90 for each flow rate, where T_{open} is the total time the glottis is open during each cycle. The phase-averaged velocity fields at each

phase are shown in Fig. 3 for a life-size flow rate of $Q_{mean} = 0.253$ L/s. The velocity magnitudes are plotted as the scaled-up experimental values. Similar plots for the other flow rates can be found in Erath and Plesniak[26] along with a more detailed description of the experimental techniques.

B. Spatial decay of the glottal jet velocity

The spatial decay of the jet core velocity as the jet moves along the vocal fold wall is extracted from the PIV data for each flow rate and phase. The extracted core velocities are fitted with the power-law profile in Eq. (9) to determine c_1, c_2, and n. The goodness of fit for the power-law provides a metric to assess the reliability of using the theoretical approach to predict the asymmetric intraglottal flow behavior.

The similarity solution discussed in Sec. II is derived in a non-inertial reference frame while the PIV data are acquired in an inertial laboratory frame. Since the vocal fold motion is prescribed and the translational and angular components as well as the center of rotation are known, the experimental velocity data can be transformed from the inertial (XYZ) to the non-inertial (xyz) frame. This is a necessary transformation in order to ensure appropriate boundary conditions upon implementation of the theoretical solution.

Velocity profiles are extracted along wall-normal planes within the glottis such that the x position is measured along the length of the wall. Data are extracted every 0.20 mm (0.01 in) along the vocal fold wall of the model. At each x position the maximum velocity is extracted and then averaged with neighboring points to reduce noise within the data. Ordered pairs for the maximum velocity are calculated at values of $x = 0.00$, 0.40, 1.40, 2.40…17.40 mm along the vocal fold wall. Data extracted in the y direction have a resolution of 0.28 mm. The distance of 17.40 mm (0.69 in) corresponds to the distance along the vocal fold wall after which the exit radius begins and the glottal area increases rapidly. This is effectively the length of the flat plate.

1. Determination of a virtual origin along plate

A power-law fit is applied to the data to determine if the decay of the free stream velocity can be expressed as

$$U(x) = c_0 x^n, \tag{12}$$

which satisfies the requirement of Eq. (9) for existence of a similarity solution with $c_0 = {c_1}^n$ and $c_2 = 0$. Equation (12) assumes that $\delta = 0$ at $x = 0$. Because a finite experimental boundary layer thickness exists at the entrance to the glottis a virtual origin for the flat plate is defined, thereby offsetting the leading edge by some distance x_{off}. After determining the thickness of the experimental boundary layer at $x = 0$, the necessary offset to ensure that the Falkner-Skan solution will have the same boundary layer thickness as the experimental value at $x = 0$ is calculated. Details of this approach are given in Erath.[25]

Accounting for the coordinate system offset, Eq. (12) becomes

$$U(x) = c_0 (x + x_{off})^n. \tag{13}$$

Over the range of investigated flow scenarios the mean value of x_{off} was 1.50 mm. The corresponding physiological value is 0.20 mm. There are four cases for which the convergence of x_{off} to a stationary value was unable to be determined: $Q_{mean} = 0.089$L/s, with $t/T_{open} = 0.90$; $Q_{mean} = 0.159$L/s with $t/T_{open} = 0.90$; and $Q_{mean} = 0.253$L/s with $t/T_{open} = 0.60$, and 0.70. There was no discernible pattern in the cases that did not converge and these cases are not used in the remainder of the analysis.

2. Estimation of free parameters

Upon determining the virtual origin of the plate for each flow scenario, the power curve fits of Eq. (13) are determined. Two representative curve fits are presented in Fig. 4. The full set of curve fits can be found in Erath.[25] The maximum deviation of the theoretical fit from the experimental data at a single point for all of the curve fits is less than 5%. The average deviation over all of the points is less than 2% for all cases. The remarkably good curve fits confirm that the

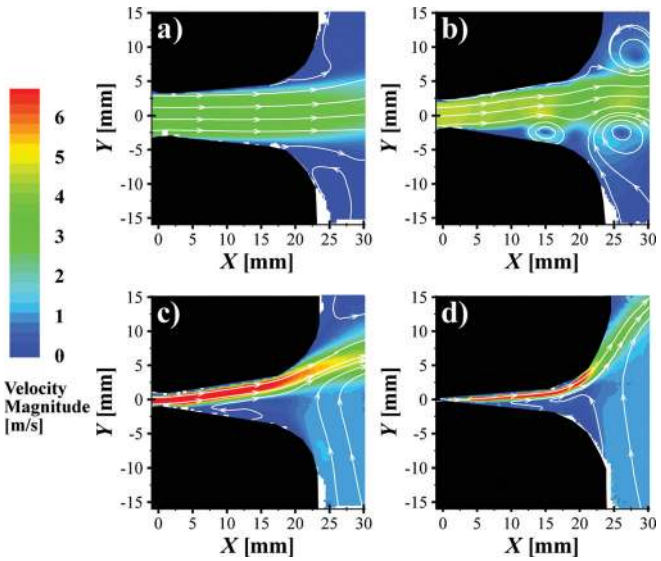

FIG. 3. (Color online) Velocity fields within the glottis of dynamically driven vocal fold models for a life-size flow rate $Q_{mean} = 0.253$ L/s at a) $t/T_{open} = 0.60$, b) $t/T_{open} = 0.70$, c) $t/T_{open} = 0.80$, and d) $t/T_{open} = 0.90$.

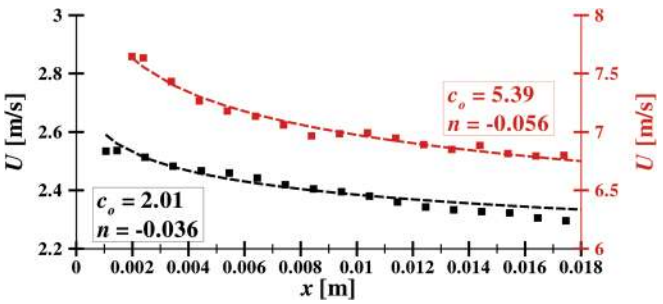

FIG. 4. (Color online) Curve fit of experimental data for $Q_{mean} = 0.159$ L/s, $t/T_{open} = 0.60$ on the left ordinate, and $Q_{mean} = 0.253$ L/s, $t/T_{open} = 0.80$ on the right ordinate.

flow behaves in a relatively self-similar manner. Values of n and β for each phonatory phase and flow rate are tabulated in Table I.

3. Falkner-Skan velocity profiles

Using the value of β from Table I, the Falkner-Skan velocity profiles are plotted and compared with the experimental data. The profiles are compared at various x locations along the plate. A representative case is presented in Fig. 5. The experimental velocity profiles are extracted at $x = 2.4$, 6.4, 10.4, and 14.4 mm. Plots for all available phases and flow rates can be found in Erath.[25]

From the values presented in Table I there is no obvious pattern in the variation of β as a function of flow rate or glottal divergence angle. The variation in the power-law exponent arises from the uncertainty in measuring the boundary-layer thickness at the glottal inlet, which in turn determines the virtual plate origin, and thereby influences the value of the exponential fit. Therefore, an average solution for all flow rates and phonatory phases that captures the bulk flow behavior when the vocal folds form a divergent channel is proposed, thereby mitigating any uncertainties that arise from estimating the boundary-layer thickness. Figure 6 compares the averaged experimental velocity profiles with the best fit Falkner-Skan profile, corresponding to $\beta = -0.03$. Comparison of the value of β from the average velocity profile with the experimental values of β in Table I shows that the best fit value ($\beta = -0.03$) is categorically larger than the experimental values, indicating a weaker adverse pressure gradient in the average case. For $\eta < 0.8$ the agreement between the Falkner-Skan profile and the averaged experimental profiles in Fig. 6 is excellent. For $\eta > 0.8$ the Falkner-Skan profile is slightly more blunt than the experimental data, though the agreement is still very good. Small discrepancies between the theoretical fit for the velocity profiles and the experimental data occur from the difficulty of determining the exact boundary layer thickness in the experimental data due to laser reflections from the vocal fold walls.

The separation point of the attached jet from the vocal fold wall is determined from the integral method of Thwaites.[56] It can be shown that flow separation is predicted at a distance greater than twice the length of the glottis for each flow scenario (phonatory phase and flow rate). Thus, it is assumed that when the flow attaches to the glottal wall it remains attached throughout the glottis and separates at the rapid area change that occurs at the glottal exit. This assumption has been confirmed by experimental observations.[26]

TABLE I. Exponents of the power-curve fits at each phase and flow rate.

Q_{mean}[L/s]	t/T_{open}	n	β
0.089	0.60	−0.038	−0.079
	0.70	−0.087	−0.190
	0.80	−0.061	−0.130
0.159	0.60	−0.036	−0.075
	0.70	−0.069	−0.150
	0.80	−0.045	−0.094
0.253	0.80	−0.056	−0.12
	0.90	−0.066	−0.140

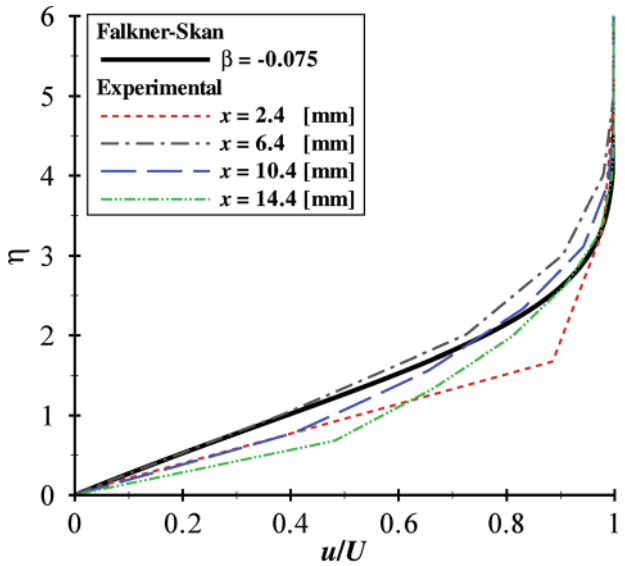

FIG. 5. (Color online) Comparison between experimentally measured velocity profiles at $x = 2.4$, 6.4, 10.4, and 14.4 mm along the glottal wall from the minimal glottal diameter with the Falkner-Skan profile at $Q_{mean} = 0.159$ L/s, $t/T_{open} = 0.60$.

C. Estimation of the intraglottal pressure distribution

Since the objective is to determine the pressure loading on the vocal fold walls, it is necessary to relate the velocity data obtained in Sec. III.B.3 to the pressure along the wall. It has been shown that there is no wall-normal pressure gradient in the boundary layer; therefore, it is only necessary to find the pressure in the inviscid core of the wall jet in the non-inertial reference frame. The resulting pressure distribution can then be impressed upon the wall and consequently incorporated into multi-mass model investigations.

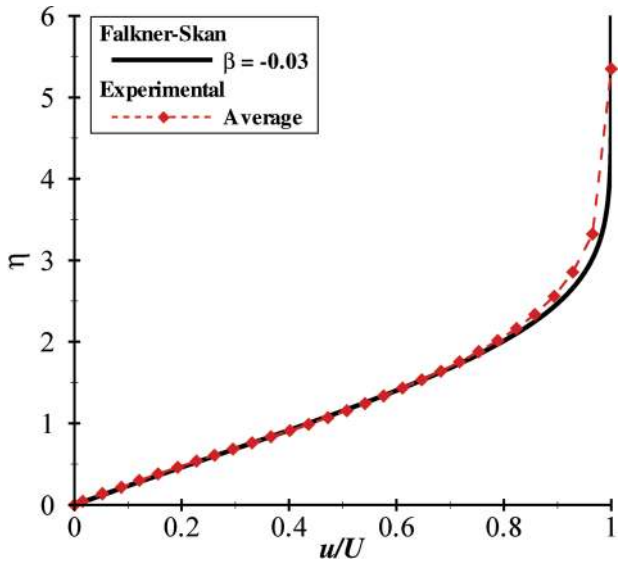

FIG. 6. (Color online) Comparison between a Falkner-Skan velocity profile with $\beta = -0.03$ and an average of the experimental velocity profiles.

Following the approach of Steinecke and Herzel[48] it is assumed that the pressure in the subglottal region, p_s, is constant and the velocity in the subglottal region is negligible, yielding $U_s = 0$. Furthermore, it is assumed that the pressure at the vocal fold exit $p_e = 0$, is atmospheric (see Fig. 7). The velocity is driven by the steady, transglottal pressure drop, where the velocity at the exit of the glottis is unknown. Finding the pressure along the flow wall requires the pressure or velocity at the minimal glottal diameter, p_i or U_i, to be known. These relations can be found by employing the previously derived boundary-layer relations prescribed by the similarity solution. Note that the minimal glottal diameter is the "inlet" to the flow model. Applying Eq. (13) at the glottal exit shows that within the boundary layer

$$U_e = c_0(x_e + x_{\text{off}})^n, \tag{14}$$

where x_e is the prescribed length of the glottis. The constant c_0 is related to the velocity at the inlet, U_i, from Eq. (12) by

$$c_0 = \frac{U_i}{x_{\text{off}}^n}. \tag{15}$$

Substituting Eq. (15) into Eq. (14) yields

$$U_e = \frac{U_i}{x_{\text{off}}^n}(x_e + x_{\text{off}})^n. \tag{16}$$

At the exit of the glottis the maximum velocity in the boundary layer is equal to the free stream velocity, by definition. If the Bernoulli equation is applied in the free stream (where it is valid because the flow is inviscid) from the inlet to the exit in Fig. 7 and Eq. (15) is substituted in for the velocity at the exit, the resulting expression can be simplified to show that

$$p_i = \frac{1}{2}\rho U_i^2\left[\left(\frac{x_e + x_{\text{off}}}{x_{\text{off}}}\right)^{2n} - 1\right], \tag{17}$$

where p_i and U_i are unknowns. Applying the Bernoulli equation from the subglottal region (p_s in Fig. 7) to the leading edge in the free stream and substituting it into Eq. (16) yields an expression for U_i as

$$U_i = \sqrt{\frac{2p_s}{\rho}}\left(\frac{x_{\text{off}}}{x_e + x_{\text{off}}}\right)^n. \tag{18}$$

The velocity U_i is now expressed entirely in terms of known parameters. Note that x_{off} is specified *a priori* as 1.50 mm from the experimental values, which corresponds to a value of 0.20 mm life-sized. Similarly, p_s must be defined *a priori*. The exponent n can be found by substituting the best fit Falkner-Skan variable of $\beta = -0.03$ into Eq. (11). The pressure at point i can now be solved from Eq. (17).

Finally, the imposed spatial pressure distribution on the flow wall is solved by applying the Bernoulli equation to the inviscid core of the glottal jet as

$$p(x) = p_i + \frac{1}{2}\rho\left[U_i^2 - U(x)^2\right], \tag{19}$$

where x is measured along the wall, with origin at the minimal glottal area, $U(x)$ is the streamwise variation in the inviscid core of the glottal jet, given by Eq. (12), and p_i and U_i are given by the boundary-layer relations of Eqs. (17) and (18), respectively.

It should be noted that this approach differs significantly from the oft-employed 1-D, inviscid Bernoulli flow solver. The 1-D Bernoulli flow solver assumes that the *entire* flow field can be described by Bernoulli's equation, neglecting viscous effects, the influence of wall motion, flow asymmetry, and flow separation (unless specified *a priori*). The BLEAP scheme applies Bernoulli's equation to certain *regions* of the flow field where Bernoulli's equation is valid (e.g., the inviscid core of the glottal jet) while relying on the boundary layer equations to prescribe the remainder of the flow field where Bernoulli's equation is not valid. Consequently, this approach does not rely upon any of the simplifying assumptions of the 1-D Bernoulli flow solver.

D. The boundary layer estimation of asymmetric pressure (BLEAP) method

A new method has been proposed for estimating the pressure distribution on the glottal walls during the divergent portion of the phonatory cycle, when the total included divergence angle is less than $-6°$ (corresponding to the experimentally observed regime of an attached glottal jet.) The method is based upon a boundary layer solution along the flow wall and thus is referred to as the Boundary Layer Estimation of Asymmetric Pressure (BLEAP) scheme. It is assumed that the flow separates from the non-flow wall at the minimal glottal diameter, hence the pressure along that wall is approximated as atmospheric. Flow remains attached to the flow wall over the length of the glottis, and separates at the glottal exit.

The proposed scheme is implemented using a two-mass model flow solver for flow through a divergent glottis via the following steps:

1. Determine the glottal geometry, including the length of the glottis, x_e.

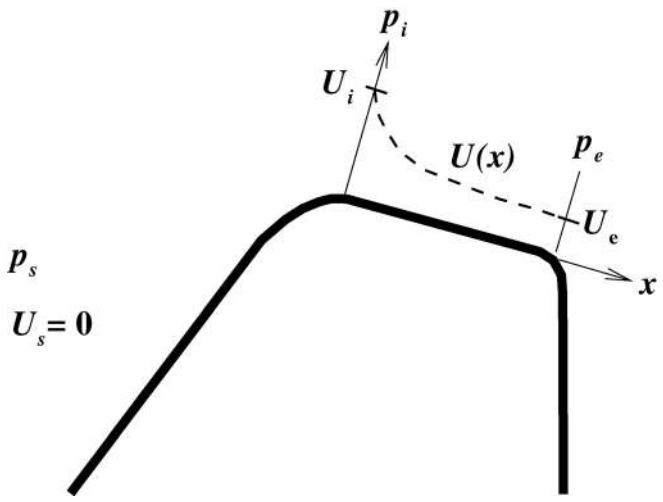

FIG. 7. Pressure and velocity variations within the glottis.

2. Specify the subglottal pressure and assume that both the subglottal velocity and exit pressure are zero.
3. Solve for the pressure and velocity at the leading edge of the flat plate portion of the glottis during the diverging portion of the phonatory cycle (point (i) in Fig. 7) by solving Eqs. (17) and (18), respectively.
4. Determine c_0 from Eq. (15).
5. Estimate the velocity decay within the glottis from Eq. (12) using $n=-0.015$ (n is obtained from Eq. (11) with $\beta=-0.03$).
6. Determine the pressure distribution along the glottal wall from Eq. (19).

The pursuit of a similarity solution proves advantageous in that it has led to the development of a scaling variable that allows the velocity decay at all flow rates and phonatory phases to be mapped by one relation. Consequently, the derived Falkner-Skan similarity solution can be broadly applied over any range of flow rates and phonatory cycles.

IV. TWO-MASS MODEL IMPLEMENTATION

The BLEAP scheme is incorporated into the vocal fold model proposed by Steinecke and Herzel,[48] referred to as SH for the remainder of the manuscript, to demonstrate the impact of the asymmetric pressure loading during the divergent portion of the phonation cycle on the vocal fold dynamics. The SH model considers each vocal fold wall to consist of two mass-spring-damper systems that are coupled via another spring, see Fig. 8.

The inferior and superior regions of the vocal folds are denoted by the subscript $j=1$ and 2, respectively, while the left and right vocal folds are described using a second subscript $\alpha=L$ and R, respectively. The mass of each vocal fold portion is $m_{j\alpha}$, spring constants are $k_{j\alpha}$, and damping parameters are $b_{j\alpha}$. The inferior and superior portions of each wall are coupled by a spring with spring constant $k_{c\alpha}$, see Fig. 8. The spring constant and damping parameter values characterize the viscoelastic tissue properties. Additional springs with spring constants $c_{j\alpha}$ are used to model the impact forces

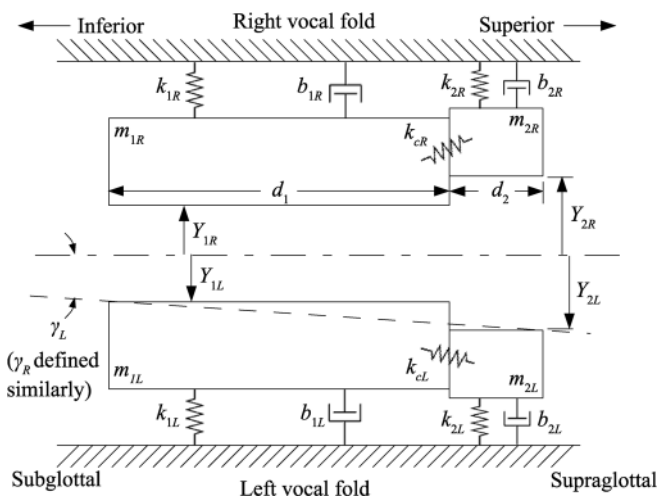

FIG. 8. Schematic of the two-mass model configuration and parameters.

generated during the collision of the left and right folds. Note that these springs are not depicted in Fig. 8 as they are only activated when the two vocal folds are in contact. To demonstrate the influence of the asymmetric pressure loading of the BLEAP scheme on the vocal fold dynamics, symmetric material properties are used, that is, $m_{jL}=m_{jR}=m_j$, $k_{jL}=k_{jR}=k_j$, $k_{cL}=k_{cR}=k_c$, $c_{jL}=c_{jR}=c_j$, and $b_{jL}=b_{jR}=b_j$. The material property values are from the "symmetric configuration" of SH. Note that despite the symmetric material properties, the left and right vocal folds can vibrate independently.

The coupled dynamical equations for the vocal fold motions are

$$m_1\ddot{Y}_{1\alpha}+b_1\dot{Y}_{1\alpha}+k_1Y_{1\alpha}+\Theta(-a_1)\frac{c_1a_1}{2l}+k_c(Y_{1\alpha}-Y_{2\alpha})=G(t), \tag{20a}$$

$$m_2\ddot{Y}_{2\alpha}+b_2\dot{Y}_{2\alpha}+k_2Y_{2\alpha}+\Theta(-a_2)\frac{c_2a_2}{2l}+k_c(Y_{2\alpha}-Y_{1\alpha})=0, \tag{20b}$$

where $Y_{j\alpha}$ is the displacement of each mass from the glottal midline (note that masses displace in the Y direction in Fig. 2), a_j is the area between the inferior or superior vocal folds, l is the length of the vocal folds in the anterior/posterior direction (the Z direction in Fig. 2), $G(t)$ is the time varying forcing function acting on the inferior glottal masses, and the dot indicates differentiation with respect to time t. The collision forces are activated when the mass displacements are negative by means of the limiting function

$$\Theta(\xi)=\begin{cases}1, & \xi>0\\ 0, & \xi\le 0.\end{cases} \tag{21}$$

In the numerical solver Θ is implemented using a hyperbolic tangent function, as prescribed by SH.[48] Following SH, it is assumed that there is no net load on the superior masses, as the pressure acting on them is assumed to always be atmospheric.

The time-varying forcing function $G(t)$ is the result of non-atmospheric pressure loading on the inferior masses and can be decomposed into opening and closing phase components, that is, $G=G_{\text{open}}+G_{\alpha,\text{close}}$. The closing phase component has a subscript α to denote that it applies to only one wall, as discussed later. During the opening phase (tile 2 of Fig. 1), the time-varying pressure within the glottis p_1 can be well approximated using the Bernoulli equation, because the pressure gradient is favorable and the boundary layers are thin. Following SH, the force on the inferior masses is symmetric and can be estimated as

$$G_{\text{open}}=ld_1p_1=ld_1p_s\left[1-\left(\frac{a_{\min}}{a_1}\right)^2\right]\Theta(a_1)\Theta(\gamma), \tag{22}$$

where the subglottal pressure, p_s, is set as 8 kPa as suggested in SH, d_1 is the length of the inferior mass in the X direction, $a_{\min}$ is the minimum glottal area, expressed as

$$a_{\min} = \max\,[0, \min(a_{1L}, a_{2L}) + \min(a_{1R}, a_{2R})], \quad (23)$$

and the glottal angle γ (see Fig. 8), is defined as

$$\gamma_L = \arctan[(Y_{1L} - Y_{2L})/(d_1 + d_2)], \quad (24)$$

$$\gamma_R = \arctan[(Y_{1R} - Y_{2R})/(d_1 + d_2)], \quad (25)$$

$$\gamma = \gamma_L + \gamma_R. \quad (26)$$

During the portions of the phonatory cycle when the glottis forms a uniform or divergent channel (tiles 3 and 4 in Fig. 1), $a_{\min} = a_1$, $\gamma \leq 0$, and thus $G_{\text{open}} = 0$. G_{open}, which will be referred to as the "opening force," is the only applied load present in the standard SH model.

During the closing phases (tile 4 of Fig. 1) the SH model assumes the flow is fully separated from both walls and thus there is no applied force on the vocal fold walls. Once the glottal angle γ reaches an angle of $-6°$ (i.e., $\gamma = -\pi/30$), the glottal jet attaches to one wall and thus a net force due to the pressure distribution is applied to one wall. This criterion is based upon experimental observation.[26,52,53] Although there is physical meaning to the specified angle, it should be noted that correlations between physical geometry and model orientations vary significantly based on the model. As such, care should be taken when relating a physical glottal angle to a model glottal angle. Note in Eq. (24) that d_2 is the length of the superior mass in the X direction. The force applied to one wall, termed hereafter the "closing force" is computed as

$$G_{\alpha,\text{close}} = \Theta(a_{\min})\Theta(-\gamma - \pi/30) \int_0^{x_e} p(x)dx, \quad (27)$$

where $p(x)$ is obtained from Eq. (19) and x_e is assumed to satisfy $x_e = d_1 + d_2$ for consistency with the experimental derivation. Equation (27) highlights a subtle point regarding the determination versus the application of the forcing functions. The loading on the vocal folds, $G(t)$, is determined by integrating the pressure distribution over the entire glottal area, as proposed by Tao.[51] The resultant forces, however, are applied only to the inferior masses $m_{1\alpha}$.

The influence of the BLEAP scheme on the radiated speech signal is studied by incorporating models of the sound fields in the subglottal and supraglottal tracts. Nonlinear flow-sound interactions are incorporated by coupling the vocal fold dynamics to wave reflection analog models for each tract. The wave reflection analog model describes the time-based propagation of one-dimensional planar acoustic waves through a collection of uniform cylindrical tubes. The implementation includes a radiation impedance at the lips, and varying loss factors for the subglottal and supraglottal tracts.[42,46] The model allows "level 1 interaction".[60] That is, the acoustic pressures interact with the glottal airflow only, and not the vocal fold dynamics.

The vocal tract area function is estimated from magnetic resonance images of an adult male sustaining the /ae/ phoneme.[61] Subglottal area functions are adapted from measurements of the trachea, bronchi, and a resistive termination, obtained from measurements performed on human cadavers.[62] The interactive acoustic model at the glottis is applied according to Titze.[63] Although the formulation of the interactive acoustic model differs slightly from the proposed flow solution, this particular acoustic model is implemented in order to allow comparison with prior investigations. This also allows the impact of asymmetric flows on the acoustic properties to be ascertained without introducing additional signal modifications arising from the application of a modified acoustic solver. A refined acoustic solver that accounts for intraglottal flow asymmetries and the effects of a time-varying outlet velocity are currently being investigated. These two components are expected to significantly increase the effects of the proposed BLEAP scheme.

The oscillation amplitudes are determined using the explicit fourth-order Runge-Kutta method with a step size of 22.68×10^{-6} s, which corresponds to a sampling rate of 44.1 kHz, in order to work in conjunction with the wave reflection analog models for each time step. The applied initial conditions force non-trivial solutions and are the same as used by SH, i.e., $Y_{1\alpha}(0) = 0.1$ cm, $\dot{Y}_{1\alpha}(0) = 0.1$ cm/ms, $Y_{2\alpha}(0) = 0$ cm, $\dot{Y}_{2\alpha}(0) = 0$ cm/ms.

A. Glottal metrics of interest

Measures of glottal behavior are computed from the minimum glottal area, glottal air-flow, and radiated sound pressure waveforms. The area-based measures include the fundamental frequency of oscillation, f_0, peak glottal area during steady state oscillation, open quotient (OQ) (ratio between open phase duration and period), speed quotient (SQ) (ratio between opening and closing phase durations), left-right (LR) amplitude asymmetry (AA) (ratio between amplitude difference and total amplitudes), and LR phase asymmetry (PA) (ratio of the time difference between the maximum lateral displacements of the left and right vocal folds and the open phase duration). These measures have been used to study soft, normal, and loud voice,[64] as well as pathological cases.[65–67]

The interactive airflow model at the glottis is used to compute peak glottal flow and maximum flow declination rate (MFDR), the latter defined as the largest negative slope of the glottal airflow waveform. The MFDR is related to vocal fold closing velocity and vocal fold trauma,[68] and is correlated with the radiated sound level for inertive vocal tract configurations.[69] The source spectral tilt is computed as the linear regression slope over the first eight harmonic peaks in the octave frequency domain of the glottal airflow.[70] An estimate of the radiated sound pressure level (SPL) at 10 cm from the lips is also obtained. The output of the wave reflection analog model after the lips is assumed to propagate as spherical waves in a free field. A Hamming window of 125 ms is used on the steady-state portion of the waveform to obtain the root-mean-squared value of the projected pressure and its logarithmic equivalent referenced to 20 μPa.

B. Numerical simulations

Two cases are explored herein: (1) repeated application of the closing force to the same vocal fold wall (arbitrarily

selected as the right wall), and (2) random selection of the vocal fold wall to which the closing force is applied, modeling cycle-to-cycle variations of the jet attachment. For both cases, the driving subglottal pressure is $p_s = 0.8$ kPa.

The results of the numerical simulations for the original symmetric two-mass model (herein referred to as 2MM), the BLEAP scheme applied only to the right vocal fold wall (referred to as B-right), and the BLEAP scheme with the attachment of the jet randomly applied to one side or the other (referred to as B-rand) are presented in Figs. 9 and 10. The results are plotted as a function of the normalized phonatory cycle, where T_{total} is the phonatory period. In Fig. 9 a comparison of the medial-lateral displacements of the inferior masses ($Y_{1\alpha}$) are presented for the 2MM, B-right, and B-rand simulations. The inset shows a zoomed-in view of the phase portrait behavior. The symmetric behavior in the 2MM case is clear from the 45° orientation of the phase portrait. When the closing force is repeatedly applied to the right vocal fold mass (see Fig. 9) the left and right vocal folds no longer vibrate symmetrically, evidenced by deviations from the symmetric case. When the closing force is randomly applied to either side the influence of the closing force on the mass displacement is evidenced by cycle-to-cycle variations in the amplitudes of the left and right inferior masses. This causes rotations in the orientation of the phase portrait where the case of B-rand in Fig. 9 shows one cycle with the flow attached to the left vocal fold.

The minimum glottal area change, volumetric flow rate, intraglottal forces (defined as the sum of the applied loads and the collision forces), and included glottal angle γ are presented in Fig. 10 for the 2MM case. The difference between the 2MM and B-right cases are plotted along the right ordinate. Results from the B-right and B-rand cases were virtually indistinguishable and consequently, only the difference for the B-right case is plotted in the figure. Figures 10(a) and 10(b) demonstrate that the closing force introduces deviations in both the glottal area and volumetric flow rate.

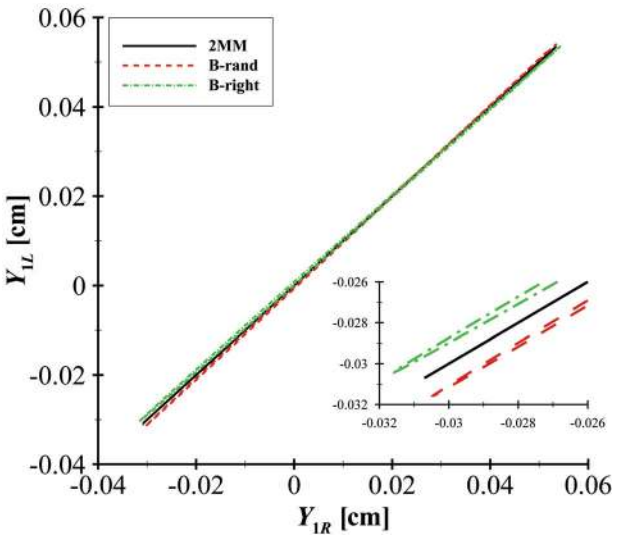

FIG. 9. (Color online) Phase portrait of the amplitude displacements for the left (Y_{1L}) and right (Y_{1R}) masses throughout a phonatory cycle. The three cases presented are for 2MM (—), B-rand (- - -), and B-right (-.-).

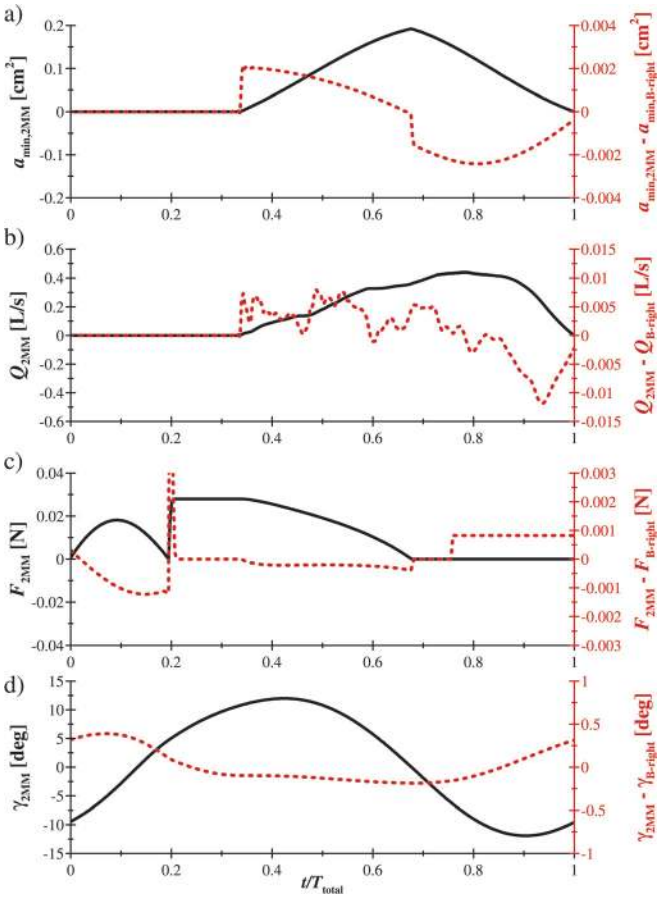

FIG. 10. (Color online) Numerical results for 2MM (—) and the difference between 2MM and BLEAP (2MM - BLEAP) (- - -) schemes showing the a) Minimum glottal area change, b) Volumetric flow rate, c) Intraglottal forces, and d) Included glottal angle for the standard 2MM versus the BLEAP implementation.

The intraglottal force is plotted in Fig. 10(c). The assumption of a symmetric, fully-separated jet regime during closing is observed for 2MM as a force with zero magnitude during closing ($t/T_{\text{total}} > 0.67$). The closing force is a constant negative force applied during the closure of the inferior mass for the BLEAP curve. Plotting the difference (2MM−B-right) results in a positive value. The negative force is constant during closure due to the underlying assumptions of multi-mass model flow behavior. The specification of a constant subglottal and supraglottal pressure casuses the velocity at the minimal glottal area to be independent of the glottal area, and therefore, to remain constant throughout the phonatory cycle. Since the asymmetric closing force is dependent on the velocity at the minimal glottal area, this simplification of the Steinecke and Herzel[48] model results in a constant closing force.

Nevertheless, a clear increase in the collision force ($0 < t/T_{\text{total}} < 0.2$) is caused by the addition of the closing force. That is, the closing force, as the name implies, increases the rate at which the vocal folds come together, causing a more forceful collision. This interaction increases the elastic forces in the system, which is largely responsible for the change in the period (see Table II). Variations in the included glottal angle (γ) throughout the phonatory cycle are presented in Fig. 10(d).

TABLE II. Results of selected glottal and acoustic metrics of interest for symmetric ($p_s = 0.8$ kPa and $Q = 1.0$), and symmetric ($p_s = 1.2$ kPa and $Q = 0.53$) vocal fold tensioning. The BLEAP scheme introduces subharmonics and has a more pronounced impact on acoustical parameters for asymmetric vocal fold tensioning.

		$p_s = 0.8$ kPa, $Q = 1.0$			$p_s = 1.2$ kPa, $Q = 0.53$		
Parameter	Units	No BLEAP	B-rand	B-right	No BLEAP	B-rand	B-right
f_0	Hz	135.9	135.9	135.9	80.1	72.7[a]	72.7[a]
L:R ratio	N.A.	1:1	1:1	1:1	1:1	3:1	3:1
SPL	dB	84.4	84.8	84.8	78.7	79.6	79.6
Peak area	cm^2	0.19	0.19	0.19	0.23	0.25	0.25
Peak flow	cm^3/s	439.3	439.7	439.7	691.4	692.6	692.8
Spectral tilt (mean)	dB/oct	−12.6	−12.4	−12.4	−12.6	−12.8	−12.8
Spectral tilt (R^2)	dB/oct	0.8	0.8	0.8	0.8	0.9	0.9
MFDR (mean)	cm^3/s^2	572.2	589.6	589.5	426.7	484.3	480.1
MFDR (σ)	cm^3/s^2	1.0	0.8	0.2	5.3	23.5	23.5
AA (mean)	%	0.0	2.5	2.8	88.0	86.3	86.5
AA (σ)	%	0.0	10.5	11.2	23.9	26.1	25.9
PA (mean)	%	0.0	0.1	0.0	49.9	35.9	36.4
PA (σ)	%	0.0	0.2	0.2	0.2	11.7	11.4
SQ (mean)	%	104.2	104.2	104.2	168.5	144.6	145.8
SQ (σ)	%	0.9	0.7	0.7	1.1	27.9	25.0
OQ (mean)	%	66.3	65.7	65.8	90.7	70.8	71.1
OQ (σ)	%	0.1	0.1	0.1	0.2	8.9	8.7

[a]Sub-harmonics present.

A quantitative description of the impact of the BLEAP scheme on the original two-mass model is obtained by computing selected glottal parameters, which are presented in Table II for two cases of symmetric vocal fold tension ($p_s = 0.8$ kPa and $Q = 1.0$) and asymmetric vocal fold tension ($p_s = 1.2$ kPa and $Q = 0.53$) where Q is the tension parameter for the model's spring, mass and damper values, as specified by Steinecke and Herzel for superior laryngeal nerve paralysis.[48] For symmetric tensioning the BLEAP scheme causes an increase in sound pressure level, spectral tilt, MFDR, and introduces asymmetries in the motion of the masses. As expected, the higher MFDR and less steep harmonic decay (i.e., harmonics with higher amplitude) yields a slightly stronger acoustic pressure output. The minor reduction in the open phase is a result of the increased closing force that pushes the vocal folds further apart during collision, thus yielding a longer closed phase.

Only the amplitude asymmetry differed between the B-rand and B-right cases. The B-rand case shows a slightly lower amplitude asymmetry than the B-right case. All other glottal parameters are the same, regardless of the side to which the jet attaches for each cycle. Surprisingly, this result suggests that the sound production arising from asymmetric flow is unaffected by whether the flow predominantly attaches to one vocal fold wall or, from cycle-to-cycle, randomly changes the wall to which it is attached.

Other parameters remain largely unaffected by the scheme, such as the fundamental frequency, peak area and glottal airflow, and speed quotient, suggesting that the BLEAP scheme has a minor effect on the tissue motion in this case. Although the current investigations were only performed for one subglottal pressure (0.8 kPa) the BLEAP scheme is expected to have an even more significant impact on the acoustic parameters as the subglottal pressure is increased, mimicking louder speech. Similar studies have shown that increasing the driving pressure increases left-right vocal fold asymmetry during vibration.[51]

When asymmetric tissue properties are considered, the influence of asymmetric pressures arising from the flow field has an increased effect on the vocal fold dynamics. Irregular vocal fold motion arises with left-to-right vocal fold oscillations occurring at a ratio of 3:1. The fundamental frequency decreases, and subharmonics emerge, evidenced by the change in left-to-right vocal fold oscillations from 1:1 to 3:1. The sound pressure level also increases by slightly more than 1 dB due to the significant increase in the MFDR. Pressure and amplitude asymmetries (PA and AA) become very significant, and large variations are also observed in the OQ and SQ. Phase portraits are shown in Fig. 11 for the case of Fig. 11(a) 2MM and Fig. 11(b) B-right. In Fig. 11(a) large asymmetries are observed in the opposing vocal fold motions, but there is still a 1:1 ratio of left and right vocal fold oscillations for each cycle. Inclusion of the BLEAP scheme, shown in Fig. 11(b), introduces period-tripling and results in a drastically modified phase portrait. The left and right vocal folds now oscillate at different frequencies such that subharmonics are generated in the oscillation cycle. A companion study focused on investigating the role of the BLEAP scheme on multi-mass models with asymmetric tissue properties is currently being performed.[71] Preliminary results have also revealed that the inclusion of more realistic "level 2"[60] acoustic interactions, where the acoustic pressure impacts the vocal fold dynamics, further augment the impact of the BLEAP solver.

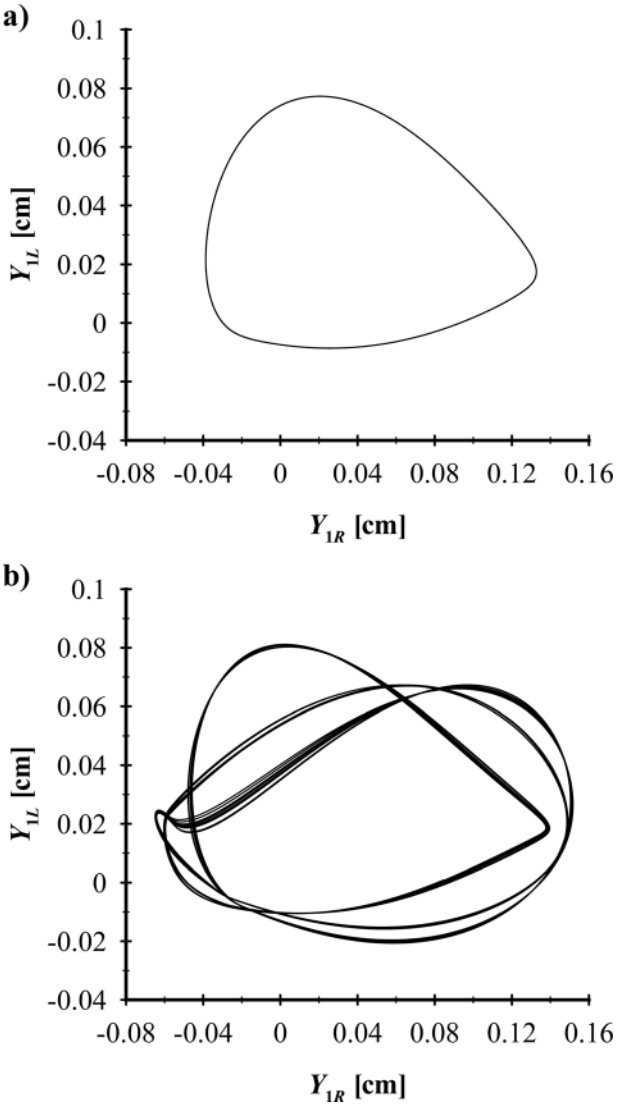

FIG. 11. Phase portraits of Y_1L versus Y_1R with $p_s = 1.2$ kPa and $Q = 0.53$ for a) 2MM and b) B-right.

V. CONCLUSIONS

A theoretical flow solver to resolve the glottal pressure loadings arising from asymmetric flow in the divergent glottis has been presented. A scaling analysis of the governing equations has shown that wall rotation acts to produce a favorable pressure gradient, delaying flow separation downstream of the origin of rotation. The validity of a Falkner-Skan similarity solution was confirmed for intraglottal flows. However, slight variations in the value of β as a function of flow rate and phonatory phase led to the proposal of an average value that provided the best fit to the averaged experimental velocity profiles. Excellent agreement was found between the theoretical and experimental profiles, with the largest amount of error arising from the difficulty in predicting the boundary layer thickness in the experimental data.

Two-mass models of the vocal folds generally assume a central jet flow regime during closure, i.e., when the glottis exhibits a divergent geometry the flow is completely detached from both walls and thus the pressure loading on the vocal fold walls is symmetric, and atmospheric. In this study, a simple method to include a force arising from asymmetric flows during the divergent portion of the glottal cycle was proposed and initially evaluated in a commonly used two-mass model of the vocal folds.

The results of the numerical simulations show that the proposed BLEAP scheme can play an important role when modeling phonation. For symmetrically-tensioned vocal folds, asymmetric pressure loading was found to have only a small influence on the glottal parameters of interest. The asymmetric pressure loadings facilitated closure, which yielded an increased maximum flow declination rate, less steep spectral tilt, and consequently, slightly higher levels of radiated sound. For the prescribed symmetric material properties, preference regarding which side of the glottis the jet attached had negligible influence on the resultant parameters. However, preliminary results indicated that the BLEAP flow solver had a much greater impact on glottal parameters when asymmetrically tensioned vocal folds were investigated, including a significant drop in fundamental frequency and the emergence of subharmonics.

Future work includes investigating time-varying expressions for the BLEAP force and introducing experimentally-based preferences in the jet trajectory. The introduction of flow inertia will modify the glottal velocity at the minimal area (whereas it is currently independent of area) and is expected to magnify the asymmetric pressures. The BLEAP scheme is also expected to have an increased influence on investigations involving more realistic "level 2" acoustic interactions. In addition, modeling asymmetric tissue properties will increase the ratio of the flow force to the tissue stiffness, thereby increasing the relative influence of asymmetric pressure loadings. Thus, the effect of asymmetric pressures on pathological conditions where asymmetries in vocal fold geometry and tissue properties are observed is expected to have a dominant influence on the nature of the asymmetric jet formation and is the focus of a companion study.

ACKNOWLEDGMENTS

This work was supported by a grant from the National Science Foundation (CBET 0828903).

[1]J. L. Flanagan, *Speech Analysis, Synthesis, and Perception*, 9-23, 2nd ed. (Springer- Verlag, New York, 1972).
[2]I. R. Titze, *Principles of Voice Production*, 87-119 (Prentice Hall, Englewood Cliffs, 1994).
[3]R. L. Wegel,"Theory of vibration of the larynx," J. Acoust. Soc. Am. 1, 1–21 (1930).
[4]R. C. Scherer, I. R. Titze, and J. F. Curtis, "Pressure-flow relationships in two models of the larynx having rectangular glottal shapes," J. Acoust. Soc. Am. **73**, 668–676 (1983).
[5]R. C. Scherer and I. R. Titze, "Pressure-flow relationships in a model of the laryngeal airway with a diverging glottis," in *Vocal Fold Physiology: Contemporary Research and Clinical Issues*, edited by D. M. Bless and J. H. Abbs, (College-Hill, San Diego, 1983) pp. 179–193.
[6]N. Binh and J. Gauffin, "Aerodynamic measurements in an enlarged static laryngeal model," Technical Report STL-QPSR 2-3, Royal Institute of Technology, Stockholm, 1983.
[7]H. M. Teager, "Some observations on oral air flow during phonation," IEEE Trans. Acoustics, Speech Signal Proc. **28**, 599–601 (1980).
[8]H. M. Teager and S. M. Teager, "The effects of separated air flow on vocalization," in *Vocal Fold Physiology*, edited by D. M. Bless and J. H. Abbs, 124–143 (College-Hill, San Diego, 1983).

[9]H. M. Teager and S. M. Teager, "Active fluid dynamic voice production models, or there is a unicorn in the garden," in *Vocal Fold Physiology: Biomechaniccs, Acoustics, and Phonatory Control*, edited by I. R. Titze and R. C. Scherer (Denver Center for the Performing Arts, Denver, 1983) pp. 387–401.
[10]J. F. Kaiser, "Some observations on vocal tract operation from a fluid flow point of view," in *Vocal Fold Physiology: Biomechaniccs, Acoustics, and Phonatory Control*, edited by I. R. Ititze and R. C. Scherer, (Denver Center for the Performing Arts, Denver, 1983) pp. 358–386.
[11]A. Hirschberg, X. Pelorson, G. C. J. Hofrmans, R. R. van Hassel, and A. P. J. Wijnands, "Starting transient of the flow through an in-vitro model of the vocal folds," in *Vocal Fold Physiology: Controlling Complexity and Chaos*, edited by P. J. Davis and N. H. Fletcher, (Singular Publishing Group, San Diego, 1996) pp. 31–46.
[12]X. Pelorson, A. Hirschberg, A. P. J. Wijnands, and H. M. A. Bailliet, "Theoretical and experimental study of quasisteady-flow separation within the glottis during phonation," J. Acoust. Soc. Am. **96**, 3416–3431 (1994).
[13]X. Pelorson, A. Hirschberg, A. P. J. Wijnands, and H. M. A. Bailliet, "Description of the flow through in-vitro models of the glottis during phonation," Act. Acust. **3**, 191–202 (1995).
[14]X. Pelorson, C. Vescovi, E. Castelli, A. Hirschberg, A. P. J. Wijnands, and H. M. A. Bailliet, "Description of the flow through in-vitro models of the glottis during phonation: Application to voiced sound synthesis," Act. Acust. **82**, 358–361 (1996).
[15]H. Coanda, "Device for deflecting a stream of elastic fluid projected into an elastic fluid," U.S. Patent No. 2,052,869, September 1, 1936.
[16]F. Alipour and R. C. Scherer, "Pulsatile airflow during phonation: An excised larynx model," J. Acoust. Soc. Am. **97**, 1241–1248 (1995).
[17]F. Alipour, V. C. Patel, and R. C. Scherer, "Measurement of pulsatile flow in excised larynges with hot-wire anemometry," ASME FED, Ind. Pap. Fluids Eng. **202**, 1–5 (1995).
[18]F. Alipour, V. C. Patel, and R. C. Scherer, "An experimental study of pulsatile flow in canine larynges," J. Fluids Eng. **117**, 577–581 (1995).
[19]B. D. Erath and M. W. Plesniak, "An investigation of bimodal jet trajectory in flow through scaled models of the human vocal folds," Exp. Fluids **40**, 683–696 (2006).
[20]B. D. Erath and M. W. Plesniak, "The occurrence of the coanda effect in pulsatile flow through static models of the human vocal folds," J. Acoust. Soc. Am. **120**, 1000–1011 (2006).
[21]B. D. Erath and M. W. Plesniak, "An investigation of jet trajectory in flow through scaled vocal fold models with asymmetrical glottal passages," Exp. Fluids **41**, 735–748 (2006).
[22]R. C. Scherer, D. Shinwari, K. J. DeWitt, C. Zhang, B. R. Kucinschi, and A. A. Afjeh, "Intraglottal pressure profiles for a symmetric and oblique glottis with a divergence angle of 10 degrees," J. Acoust. Soc. Am. **109**, 1616–1630 (2001).
[23]R. C. Scherer, D. Shinwari, K. J. DeWitt, C. Zhang, B. R. Kucinschi, and A. A. Afjeh, "Intraglottal pressure profiles for a symmetric and oblique glottis with a uniform duct," J. Acoust. Soc. Am. **112**, 1253–1256 (2001).
[24]D. Shinwari, R. C. Scherer, K. J. DeWitt, and A. A. Afjeh, "Flow visualization and pressure distributions in a model of the glottis with a symmetric and oblique divergent angle of 10 degrees," J. Acoust. Soc. Am. **113**, 487–497 (2003).
[25]B. D. Erath, "An experimental and theoretical assessment of flow asymmetries in normal and pathological speech," Ph.D. thesis, 1–281, Purdue University, West Lafayette, 2009.
[26]B. D. Erath and M. W. Plesniak, "An investigation of asymmetric flow features in a scaled-up model of the human vocal folds," Exp. Fluids **49**, 131–146 (2010).
[27]B. D. Erath and M. W. Plesniak, "Viscous flow features in scaled-up physical models of normal and pathological phonation," Int. J. Heat Fluid Flow **31**, 468–481 (2010).
[28]B. R. Kucinschi, R. C. Scherer, K. J. DeWitt, and T. T. M. Ng, "Coherent structures of the near field flow in a self-oscillating physical model of the vocal folds," Trans. ASME, J. Biomech. Eng. **128**, 380–390 (2006).
[29]B. R. Kucinschi, R. C. Scherer, K. J. DeWitt, and T. T. M. Ng, "An experimental analysis of the pressures and flow within a driven mechanical model of phonation," J. Acoust. Soc. Am. **119**, 3011–3021 (2006).
[30]M. H. Krane, M. Barry, and T. Wei, "Unsteady behavior of flow in a scaled-up vocal folds model," J. Acoust. Soc. Am. **122**, 3659–3670 (2007).
[31]J. Neubauer, Z. Zhang, R. Miraghie, and D. Berry, "Coherent structures of the near field flow in a self-oscillating physical model of the vocal folds," J. Acoust. Soc. Am. **121**, 1102–1118 (2007).
[32]J. S. Drechsel and S. L. Thomson, "Influence of supraglottal structures on the glottal jet exiting a two-layer synthetic, self-oscillating vocal fold model," J. Acoust. Soc. Am. **123**, 4434–4445 (2008).
[33]B. A. Pickup and S. L. Thomson, "Influence of asymmetric stiffness on the structural and aerodynamic response of synthetic vocal fold models," J. Biomech. **42**, 2219–2225 (2009).
[34]S. M. Khosla, S. Murugappan, E. J. Gutmark, and R. C. Scherer, "Vortical flow field during phonation in an excised canine larynx model," Ann. Otol. Rhinol. Laryngol. **116**, 217–228 (2007).
[35]J. L. Flanagan and L. L. Landgraf, "Self-oscillating source for vocal tract synthesizers," IEEE Trans. Audio Electroacoust. **AU-16**, 57–64 (1968).
[36]K. Ishizaka and J. L. Flanagan, "Synthesis of voice sounds from a two-mass model of the vocal cords," Bell Sys. Tech. J. **51**, 1233–1268 (1972).
[37]F. Avanzini, P. Alku, and M. Karjalainen, "One-delayed-mass model for efficient synthesis of glottal flow," EuroSpeech Conf. Proc. 51–54 (2001).
[38]J. Horacek and J. G. Svec, "Aeroelastic model of vocal-fold-shaped vibrating element for studying the phonation threshold," J. Fluids Struct. **16**, 931–955 (2002).
[39]J. Horacek and J. G. Svec, "Instability boundaries of a vocal fold modeled as a flexibly supported rigid body vibrating in a channel conveying fluid," Proc. IMECE 2002, 1–12 (2002).
[40]M. Kob, "Physical modeling of the singing voice," Ph.D. thesis, University of Technology Aachen, Berlin, Germany, 2002.
[41]J. C. Lucero, "Oscillation hysteresis in a two-mass model of the vocal folds," J. Sound Vib. **282**, 1247–1254 (2005).
[42]B. H. Story and I. R. Titze, "Voice simulation with a body-cover model of the vocal folds," J. Acoust. Soc. Am. **97**, 1249–1260 (1995).
[43]T. Wurzbacher, R. Schwarz, M. Döllinger, U. Hoppe, U. Eysholdt, and J. Lohscheller, "Model-based classification of nonstationary vocal fold vibrations," J. Acoust. Soc. Am. **120**, 1012–1027 (2006).
[44]H. Teffahi, "A two-mass model of the vocal cords: Determination of control parameters," Proc. Int. Conf. Multimedia Comput. Syst. **9**, 87–90 (2009).
[45]N. Ruty, X. Pelorson, A. Van Hirtum, I. Lopez-Arteaga, and A. Hirschberg, "An in vitro setup to test the relevance and accuracy of low-order vocal fold models," J. Acoust. Soc. Am. **121**, 479–490 (1997).
[46]M. Zañartu, L. Mongeau, and G. R. Wodicka, "Influence of acoustic loading on an effective single mass model of the vocal folds," J. Acoust. Soc. Am. **121**, 1119–1129 (2007).
[47]J. van den Berg, J. Zantema, and P. Doornenbal, "On the air resistance and bernoulli effect of the human larynx," J. Acoust. Soc. Am. **29**, 626–631 (1957).
[48]I. Steinecke and H. Herzel, "Bifurcations in an asymmetric vocal-fold model," J. Acoust. Soc. Am. **97**, 1874–1884 (1995).
[49]Z. Zhang, J. Neubauer, and D. A. Berry, "Physical mechanisms of phonation onset: A linear stability analysis of an aeroelastic continuum model of phonation," J. Acoust. Soc. Am. **122**, 2279–2295 (2007).
[50]J. C. Lucero, "Optimal glottal configuration for ease of phonation," J. Voice **12**, 151–158 (1999).
[51]C. Tao, Y. Zhang, D. G. Hottinger, and J. J. Jiang, "Asymmetric airflow and vibration induced by the coanda effect in a symmetric model of the vocal folds," J. Acoust. Soc. Am. **122**, 2270–2278 (2007).
[52]R. W. Fox and S. J. Kline, "Flow regime data and design methods for curved subsonic diffusers," J. Basic Eng., Trans. ASME **84**, 303–312 (1962).
[53]C. R. Smith and S. J. Kline, "An experimental investigation of the transitory stall regime in two-dimensional diffusers," J. Fluids Eng. **96**, 11–15 (1974).
[54]A. G. Hansen, *Similarity Analyses of Boundary Value Problems in Engineering*, (Prentice-Hall, Englewood Cliffs, 1964).
[55]M. B. Glauert, "The wall jet," J. Fluid. Mech. **1**, 625–643 (1956).
[56]F. M. White, *Viscous Fluid Flow*, 239–245 (McGraw-Hill, New York, 2006).
[57]K. N. Stevens, *Acoustic Phonetics*, 27–37 (MIT press, Cambridge, 1998).
[58]V. M. Falkner and S. W. Skan, "Some approximate solutions of the boundary layer equations," Philos. Mag. **12**, 865–896 (1931).
[59]R. L. Panton, *Incompressible Flow*, 593–599 (John Wiley, New York, 1996).
[60]I. R. Titze, "Nonlinear source-filter coupling in phonation: Theory," J. Acoust. Soc. Am. **123**, 2733–2749 (2008).

[61]B. H. Story, I. R. Titze, and E. A. Hoffman, "Vocal tract area functions from magnetic resonance imaging," J. Acoust. Soc. Am. **100**, 537–554 (1996).
[62]E. R. Weibel, *Morphometry of the Human Lung,* **139**, first edition (Springer, New York, 1963).
[63]I. R. Titze, "Parameterization of the glottal area, glottal flow, and vocal fold contact area," J. Acoust. Soc. Am. **75**, 570–580 (1984).
[64]E. B. Holmberg, R. E. Hillman, and J. S. Perkell, "Glottal airflow and transglottal air pressure measurements for male and female speakers in soft, normal, and loud voice," J. Acoust. Soc. Am. **84**, 511–529 (1988).
[65]J. G. Švec, F. Šram, and H. K. Schutte, "Videokymography in voice disorders: What to look for?," Ann. Otol. Rhinol. Laryngol. **116**, 172–180 (2007).
[66]H. S. Bonilha, D. D. Deliyski, and T. T. Gerlach, "Phase asymmetries in normophonic speakers: Visual judgments and objective findings," Am. J. Speech Lang. Pathol. **17**, 367–376 (2008).
[67]D. D. Mehta, D. D. Deliyski, S. M. Zeitels, and R. E. Hillman, "Voice production mechanisms following phonosurgical treatment of early glottic cancer," Ann. Otol. Rhinol. Laryngol. **119**, 1–9 (2010).
[68]R. E. Hillman, E. B. Holmberg, J. S. Perkell, M. Walsh, and C. Vaughan, "Objective assessment of vocal hyperfunction: An experimental framework and initial results," J.Speech Hear. Res. **32**, 373–392 (1989).
[69]I. R. Titze, "Theoretical analysis of maximum flow declination rate versus maximum area declination rate in phonation,"J. Speech Lang. Hear. Res. **49**, 439–447 (2006).
[70]S. Murugappan, S. Khosla, K. Casper, L. Oren, and E. Gutmark, "Flow fields and acoustics in a unilateral scarred vocal fold model," Ann. Otol. Rhinol. Laryngol. **118**, 44–50 (2009).
[71]B. D. Erath, M. Zañartu, S. D. Peterson, and M. W. Plesniak, "Nonlinear vocal fold dynamics resulting from asymmetric fluid loading on a two-mass model of speech," Chaos, (submitted).